

# Event-Based De-Snowing for Autonomous Driving

Manasi Muglikar

Nico Messikommer

Marco Cannici

Davide Scaramuzza

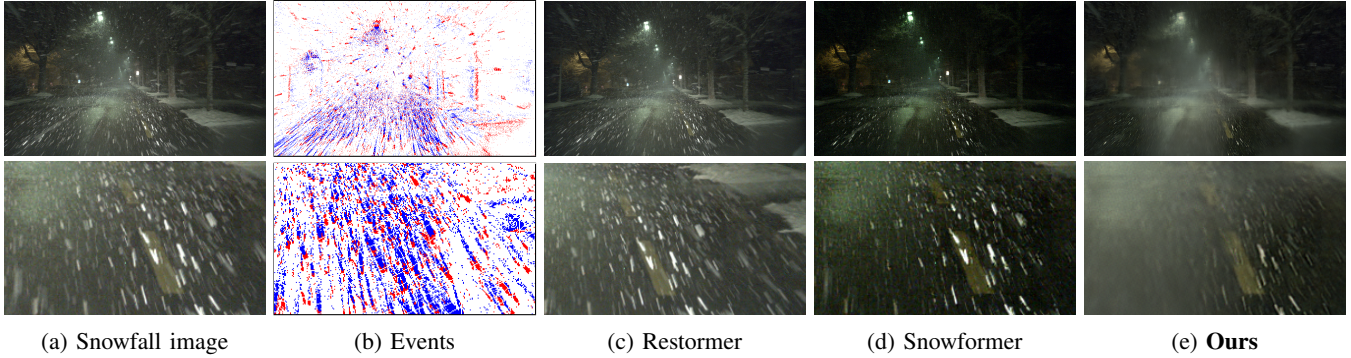


Fig. 1: **Event-based video snow removal in challenging nighttime scenes:** (a) Sample image from our dataset captured while driving in snowfall, and (b) corresponding event data highlighting the motion of snowflakes. The presence of dense, dynamic snow and low visibility presents significant challenges for conventional image restoration methods, as illustrated by the results of (c) Restormer [1] and (d) Snowformer [2]. Our proposed event-based approach (e) utilizes event information to address these challenges and restore clearer scene content under adverse weather conditions.

**Abstract**—Adverse weather conditions, particularly heavy snowfall, pose significant challenges to both human drivers and autonomous vehicles. Traditional image-based de-snowing methods often introduce hallucination artifacts as they rely solely on spatial information, while video-based approaches require high frame rates and suffer from alignment artifacts at lower frame rates. Camera parameters, such as exposure time, also influence the appearance of snowflakes, making the problem difficult to solve and heavily dependent on network generalization. In this paper, we propose to address the challenge of desnowing by using event cameras, which offer compressed visual information with submillisecond latency, making them ideal for de-snowing images, even in the presence of ego-motion. Our method leverages the fact that snowflake occlusions appear with a very distinctive streak signature in the spatiotemporal representation of event data. We design an attention-based module that focuses on events along these streaks to determine when a background point was occluded and use this information to recover its original intensity. We benchmark our method on DSEC-Snow, a new dataset created using a green-screen technique that overlays pre-recorded snowfall data onto the existing DSEC driving dataset, resulting in precise ground truth and synchronized image and event streams. Our approach outperforms state-of-the-art de-snowing methods by 3 dB in PSNR for image reconstruction. Moreover, we show that off-the-shelf computer vision algorithms can be applied to our reconstructions for tasks such as depth estimation and optical flow, achieving a 20% performance improvement over other de-snowing methods. Our work represents a crucial step towards enhancing the reliability and safety of vision systems in challenging winter conditions, paving the way for more robust, all-weather-capable applications.

**Video** <https://youtu.be/9FneWDDwQ8E>

This work was supported by the European Research Council (ERC) under grant agreement No. 864042 (AGILEFLIGHT). The authors are with the Robotics and Perception Group, Department of Informatics, University of Zurich, Switzerland.

## I. INTRODUCTION

Imagine driving through heavy snowfall. Bright, swirling flakes, windshield accumulation, and reduced visibility severely degrade scene perception, making driving not only unpleasant but also potentially dangerous. Autonomous vehicles and assistive driving systems, designed to enhance road safety, also struggle in these conditions as snowflakes obscure both camera and LiDAR sensors. To advance vehicle autonomy and automotive safety, addressing adverse weather challenges is crucial. Thus, effective de-snowing techniques are necessary to ensure the reliability and safety of vision systems in snowy environments.

Existing solutions, such as training a network on specific de-snowing datasets [3], [4], [5], [6], [7], [8] or using Gated Cameras [3], fall short—either failing to generalize across snow conditions or losing intensity information in low light. In comparison to a single image, a video provides richer temporal context about the dynamic features of the scene. Building on this, existing works [3], [8], [9], [10], [11], [12], [13], [14] have studied the effect of incorporating this temporal information for image de-snowing, showing promising results. However, the performance of video de-snowing relies on the framerate of the camera. A high framerate ensures reliable alignment across individual frames, which can be used to align the background and remove snow occlusion. For effective image de-snowing, it is crucial to capture high-speed scene information. We, therefore, propose to solve this problem by using event cameras, which provide extremely high temporal resolution (on the order of 1 MHz), without a huge bandwidth demand.

Event cameras measure intensity changes with very low latency (up to 1  $\mu$ s) and asynchronously [15]. This produces a stream of events that encode the time, location, and polarity of

the brightness change. The main advantages of event cameras include sub-millisecond latency, very high dynamic range ( $> 120$  dB), and strong robustness to motion blur. This work leverages these unique properties to remove snow occlusions from images effectively.

Since event cameras have high temporal resolution and no exposure time, snowflakes always appear as streaks in the space-time representation of events (c.f. Fig. 2). This is unlike conventional cameras, where the exposure time plays a major role in the appearance of the snowflake. Thus, our method takes advantage of this unique signature in the space-time domain to track these streaks. In the absence of ego-motion, the task of recovering background intensity is quite simple, as one only has to look at the intensity changes (or events) per pixel. However, with ego-motion, the point corresponding to the pixel that is occluded at a certain time may not be the same at a future time. Therefore, keeping track only along the pixel will result in significant errors. Instead, we propose to look along the streak, as a point in 3D space will be occluded and de-occluded along this streak. To recover the background intensity where the occlusion covers the background, it is necessary to look along the streak in time. By focusing only on points along these streaks, we can accurately determine when a point in the scene was occluded. Using this information, we reconstruct the background intensity, enabling us to recover a clear image even under challenging weather conditions. Our approach improves the performance of image-based and video-based approaches by over 3 dB in terms of PSNR of image reconstruction. Not only that, we also outperform image-based approaches in further downstream tasks such as depth estimation, optical flow, and object detection by over 20% in terms of accuracy.

We list our contributions as follows:

- **A new event-based de-snowing dataset generated by chroma composition method:** We develop a synthetic dataset (DSEC-Snow) by overlaying recorded snowfall onto the DSEC [16] driving dataset using green-screen technology, providing precise ground truth and synchronized image-event streams without the need for complex snow rendering.
- **A novel approach for de-snowing images using event cameras:** Our approach utilizes the rich temporal information of events to detect and remove snowflake occlusions by tracking their spatiotemporal streaks, enabling accurate background recovery. We also propose a simple learning framework to fuse the event and image information for improved de-snowing performance.
- **A real-world driving dataset collected in snowy conditions:** We present a real-world event-camera dataset captured while driving in snowfall, offering valuable data for testing the robustness of event-based de-snowing methods in practical scenarios.

## II. RELATED WORK

We summarize the related works for image and video desnowing in Section II-A. There has been some progress in the context of image deraining with event cameras, which

Dataset	Simulation	Sensors	GT
Snow100K [4]	Yes	Image	Yes
SnowCityScapes [5]	Yes	Image	Yes
SnowKITTI2012 [5]	Yes	Image	Yes
SRRS [6]	Yes	Image	Yes
CSD [7]	Yes	Image	Yes
SnowVideo [8]	Yes	Video	Yes
<b>DSEC-Snow (ours)</b>	Yes	Video + Events	Yes
<b>SnowDriving (ours)</b>	No	Video + Events	No

TABLE I: **Comparison of snow datasets.** Existing snow datasets primarily focus on synthetic image-based data with ground truth (GT), while our DSEC-Snow and SnowDriving datasets provide real and simulated video sequences with event data, addressing the need for benchmarks suitable for event-based snow removal under more realistic conditions

is summarized in Section II-B. Lastly, we also summarize the existing datasets published so far for image desnowing in Section II-C.

### A. Image and video de-snowing

Estimating the background image in the presence of rain or snow is challenging as it requires hallucination of the background content. Some earlier works focused on modeling the rain streaks and snowflakes and decomposed the image into background and foreground components [17], [18]. However, even if the perfect model of the rain streaks or snowflakes is known, the background content is still challenging to estimate [19]. To address this issue, recent works [4], [6] have proposed using deep learning methods to estimate the background content. [5] proposed learning a representation for snow using the geometric and semantic properties of snow. On the other hand, Snowformer [2] proposes using a vision transformer that fully combines local and global information and obtains state-of-the-art results. Other image-based approaches focus more on image restoration [1] or image deraining [20], both of which do not generalize well for image desnowing [8]. Recent work [20] tackles the unique challenges of nighttime deraining—caused by non-uniform local illumination and complex rain-light interactions—by introducing a Rain Location Prior (RLP) learned via a recurrent residual model, along with a Rain Prior Injection Module (RPIM) to enhance feature representation and boost deraining performance at night. Instead of handling each image restoration task separately, Restormer [1] proposes a unified framework for image restoration tasks, including image deraining, deblurring, and denoising. However, the performance of a generalized image restoration method is often limited for specialized tasks such as image desnowing. Therefore, Snowformer [2] proposes a dedicated desnowing vision transformer with a scale-aware snow query and local-patch embedding, resulting in state-of-the-art results for image desnowing. These methods, however, rely on the spatial information available in the image to estimate the background content. In complex weather conditions, such as heavy snowfall, the spatial information is often not sufficient to accurately estimate the background content.

Increasing temporal resolution for this task gives rise to video-based desnowing methods. Video-based desnowing

methods [9] have explored the use of temporal information to improve the quality of desnowed images. The seminal work of Garg et al. [9] proposed a model-based approach to remove occlusions such as rain by characterizing the photometric and temporal properties of rain streaks. Subsequent works [21], [22], [23], [24], [25] have extended this work by proposing various priors to model the rain streaks and snowflakes. Another line of approach used matrix factorization to encode the correlation of background video along the temporal dimension [14], [26], [27], [28].

More recently, deep learning methods have also shown significant improvements in video desnowing [8], [29], [30], [31], [32], [33], [34], [35]. Li et al. [29] proposed a multi-scale convolutional neural network (CNN) for sparse coding to encode and remove the repetitive local patterns of rain streaks at different scales. Liu et al. [31] proposed a recurrent neural network (RNN) to turn this problem into classification of rain pixels and then recover the background. While these methods have shown promising results on synthetic data, they often struggle with complex weather conditions and fail to generalize to real-world scenarios. To address the domain gap between synthetic and real rain data, recent work [35] proposes a semi-supervised video deraining method that leverages a deep-learning-based dynamical rain generator and Monte Carlo EM optimization, jointly exploiting both labeled synthetic and unlabeled real videos for improved performance in real-world scenarios. Recently, Chen et al. [8] addressed the challenging task of video snow removal by introducing a high-quality dataset that simulates realistic snow and haze through advanced rendering and augmentation techniques.

### B. Event-based image deraining

Event cameras, known for their high temporal resolution and robustness to motion blur, have been increasingly utilized to enhance traditional imaging systems [36], [37]. This high temporal resolution of events was used for de-occluding frames [38]. This technique utilizes the asynchronous nature of event cameras to provide additional temporal information, enabling more effective de-occlusion of images in real-time scenarios.

Similarly, [39] introduced an unsupervised video deraining method that combines event data with traditional video frames. By integrating these two data types, the method effectively removes rain streaks and other occlusions from video sequences, demonstrating significant improvements in visibility and clarity.

### C. Snow Datasets

While there has been significant progress in the field of image and video desnowing, the availability of datasets for training and evaluating these methods remains limited. Some existing datasets focus on image desnowing, such as Snow100K [4], which provides a large collection of synthetic images with snow occlusions generated using Photoshop rendering techniques [40], providing ground truth images. In SnowKITTI2012 and SnowCityScapes [5], the authors used a similar approach to generate different densities of snow occlusions on images. SRRS [6], [7] improved these models

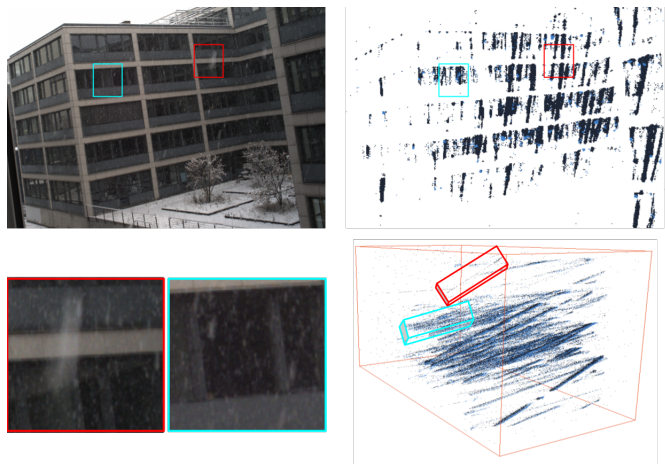


Fig. 2: **Effect of snow on images (left) and events (right)** (Left) The appearance of snowfall in an image depends on multiple factors, such as snowflake size, density, ambient illumination, and camera exposure settings. Two such examples are shown within the red and blue regions. (Right) The same snow occlusions in event data are visualized on the image plane and x-y-t volume (bottom-right). Irrespective of the snowflake size, snow occlusions have a unique spatio-temporal pattern in the form of streaks (bottom-right).

and included more realistic rendering of snowy scenes by introducing a veiling effect and then using Photoshop to render snowflakes. Since these datasets rely on Photoshop, the realism of the snow occlusions is lacking, and therefore causes limited generalization to real-world desnowing of images. Therefore, [8] proposed a new video desnowing dataset which is rendered using Unreal Engine, providing a more realistic simulation of snow occlusions. These datasets, however, do not provide events. A comparison of these datasets is shown in Table I.

To the best of our knowledge, there currently exists no dataset that provides events and images for the task of desnowing. We therefore propose two datasets for this task, namely the DSEC-Snowdataset and Slider-SnowDataset. The DSEC-Snowdataset overlays foreground data of snowfall recorded with an event camera onto a background consisting of the driving dataset DSEC [16]. This process removes the complexity of rendering snow particles that are both photo-realistic and physically accurate. Another advantage this dataset provides is the availability of synchronized events, images, and ground truth images. In addition to this, we also record real data of driving in snowfall using a color DAVIS event camera, called Slider-Snow.

## III. UNDERSTANDING THE EFFECT OF SNOW ON IMAGES AND EVENTS

The appearance of snow in images and events is quite different due to the nature of the sensors. Garg et al. [9] analyzed snowflakes and showed that their appearance depends not only on the size, shape, and distance from the camera, but also on the ambient illumination and camera exposure settings. This results in a wide variety of snowflake appearances in images, as shown in Fig. 2 (top). For example, [9] provided a

---

**Algorithm 1** Background intensity estimation under snow occlusion using event data.

---

*Input:* Stream of polarity events  $p(t)$  triggered by snowflake occlusions at pixel  $X$ , snowflake intensity  $I_r$ , contrast threshold  $C$ , time window  $\tau$ , [optional] warping function  $W(\cdot)$ .

*Output:* Estimated background intensity  $I_b$  at each pixel  $X$ .

*Procedure:*

Initialize background intensity estimate:  $I_b \leftarrow I_r$

**Case 1: Static Background**

Accumulate event polarity over  $\tau$ :  $E = \int_0^\tau p(t) dt$

Update background intensity:  $I_b \leftarrow I_r - C \times E$

**Case 2: Background with Motion**

Identify warping  $W(\cdot)$  along motion streaks (e.g., using velocity prior)

Warp events:  $E_w = \int_0^\tau W(p(t) \times C) dt$

Update background intensity:  $I_b \leftarrow I_r - E_w$

**return**  $I_b$

---

mathematical model of how snow can appear either as bright spots, streaks, or even haze depending on the distance of the snowflake from the camera, for the same exposure settings. This makes the challenge of identifying snowflakes in images quite significant.

On the other hand, snow occlusions in event data have a unique spatio-temporal pattern in the form of streaks, as shown in Fig. 2 (bottom). This is because of the high temporal resolution of the event camera, which captures the snow occlusions as streaks in the x-y-t volume. This makes the task of identifying snow occlusions in events much easier compared to images. The streaks in the x-y-t volume are independent of the distance and only depend on the relative difference between background intensity and snowflake intensity. For example, in Fig. 2 (bottom, left), the snow streak corresponding to the same snowflake is visible in front of a darker background like the window, but not visible in front of a brighter background like the sky. This makes the task of identifying snow occlusions in events much easier compared to images.

*A. De-occluding with events*

We now describe a geometric way to solve for background extraction using events. This algorithm is also summarized in 1. As a snowflake moves in front of the background, it causes an intensity change, resulting in events being triggered. The intensity at a pixel  $\mathbf{X}$  at time  $t$  caused by a snowflake of intensity  $I_r$  occluding a background intensity of  $I_b$  can be written as:

$$\Delta I(t) = I_r - I_b = pC \quad (1)$$

In general, since the snowflake is usually brighter than the background, the intensity change is positive when the snowflake is occluding the background, triggering positive polarity events. When the snowflake moves away from the

background, the intensity change is negative, triggering negative polarity events. Therefore, assuming we know the intensity of the snowflake, estimating the background intensity is simply a matter of integrating the events over time  $\tau$ , scaling it by the contrast threshold  $C$ , and subtracting it from the snowflake intensity. Thus, the background intensity can be estimated as:

$$I_b = I_r - \sum_0^\tau pC \quad (2)$$

Therefore, once we have identified the snow occlusions (using events), we can recover the background intensity from the equation above and attend to events that occur at the same pixel at different times. In the presence of background motion, Equation. 2 no longer holds true, as the pixel before and after the occlusion can belong to a different point. This implies that the pixel at location  $X_0$  being occluded at time  $t_0$  could be at location  $X_i$  when it is de-occluded. Therefore, the search for the corresponding de-occluded pixel is no longer only along the time dimension but also along the spatial dimension. What does remain true, however, is that the equation still holds in 3D space, and the above equation is modified as follows:

$$I_b = I_r - \sum_0^\tau W(pC) \quad (3)$$

Here,  $W$  represents the warping of events along the motion streak. However, estimating this warp is quite challenging, especially when the snow occlusions are dense and overlapping. We follow the approach of [9] to identify the streaks using the rain-velocity prior and use this to recover the background intensity. The main difference with respect to [9] is that we use events instead of a set of images as input to this method. This forms our model-based approach to de-occlude the snow occlusions in images using events. As this approach requires several assumptions about the snow occlusions, we also propose a data-driven approach to learn to de-occlude the snow occlusions using events, which we describe in the following sections.

IV. DATA-DRIVEN DE-SNOWING WITH EVENT CAMERAS

In this section, we present our approach for de-snowing images using event cameras. Our method leverages a data-driven network architecture that learns to de-occlude images affected by transient occlusions using both intensity images and event data. The design of each component is inspired by classical geometric approaches but replaces explicit modeling with learnable modules. An overview of our proposed method is shown in Fig. 3.

Our approach consists of three main components: (1) **EventNet**, which processes the event stream to extract spatio-temporal patterns of snowflake streaks; (2) **Image Reconstruction**, which fuses the image and event features using a transformer; and (3) **Adaptive Fusion**, which reconstructs the clean image by combining the network prediction and the input image guided by a learned mask.

**EventNet** The EventNet module is designed to extract spatio-temporal features from the raw event data, which encode the motion and geometry of snowflake occlusions.

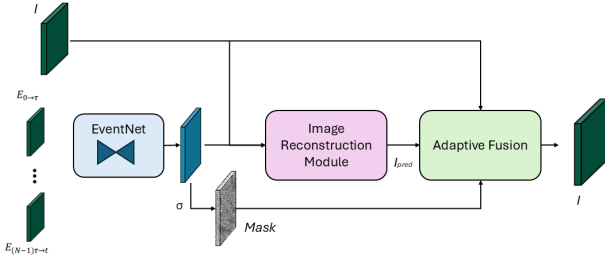


Fig. 3: **Overview of our data-driven method for reconstructing deoccluded images using event-camera data.**

Events within the camera’s exposure time are segmented into non-overlapping spatio-temporal windows, converted into voxel-grid representations, and processed alongside RGB images through modality-specific feature extraction. Event features are extracted via EventNet, which also produces a spatial mask. The image reconstruction module fuses event and image features to generate a prediction, and adaptive fusion leverages the learned mask to combine the prediction and the original image, resulting in a de-occluded output.

Instead of relying on explicit warping or velocity priors as in classical geometric models, EventNet employs a convolutional LSTM (ConvLSTM) to capture temporal dependencies, followed by a U-Net architecture for hierarchical spatial feature extraction. This structure enables the network to implicitly learn the geometric properties of snow streaks from data. The output feature map is further used to generate a spatial mask by channel-wise summation and sigmoid activation, indicating the likelihood of occlusion at each pixel. This mask serves as a soft, learnable analog to the explicit identification of occlusions in geometry-based approaches.

**Image Reconstruction** The image reconstruction module uses a hierarchical Transformer-based architecture proposed in Snowformer [2]. This Transformer fuses features from both the intensity image and the processed event stream. It comprises a U-Net-style encoder-decoder structure built upon Transformer blocks, which are capable of capturing long-range dependencies and aggregating contextual information across multiple scales. Channel attention mechanisms and context interaction layers further enhance feature fusion at each scale.

It replaces hand-crafted priors and explicit motion modeling with multi-head self-attention and hierarchical feature aggregation, allowing the network to learn complex, non-linear dependencies across both spatial and temporal domains. The Transformer’s ability to capture global context serves as a learnable analog to geometric reasoning over motion and occlusion structure, integrating information from both local neighborhoods and the entire image

**Adaptive Fusion** In the final stage, we perform an adaptive, pixel-wise fusion between the input image and the network’s de-snowed prediction. The fusion is controlled by the learned spatial mask generated by EventNet:

$$\hat{I} = \text{mask} \odot I_{\text{pred}}(x) + (1 - \text{mask}) \odot I_{\text{input}}, \quad (4)$$

where  $I_{\text{pred}}(x)$  is the output of the Transformer backbone,

$I_{\text{input}}$  is the original input image, and  $\text{mask}$  is the spatial mask produced by EventNet. The operator  $\odot$  denotes element-wise multiplication.

This formulation can be interpreted as a data-driven generalization of the subtraction operation in geometry-based approaches, where the mask adaptively determines the contribution of the predicted clean image and the original input. Rather than explicitly subtracting a warped occlusion estimate (as done in model-based approach), the network learns the optimal blending strategy for each pixel, guided by the inferred occlusion geometry from the event data.

#### A. Input Representation

Our method operates on two complementary modalities: standard images and event data that are synchronized and aligned with each other. The input image is represented as a conventional three-channel RGB tensor. The events correspond to all illumination changes that occur within the exposure time of the camera. Events are encoded into a voxel grid representation with  $B$  temporal bins along the channel dimension, effectively capturing the spatio-temporal structure of event streams in a fixed-size tensor.

#### B. Loss Function

For training supervision, we adopt the **L1 loss** as our primary reconstruction loss. The loss function is defined as:

$$L_{L1} = \|S(I(x)) - Y\|_1, \quad (5)$$

where  $S(\cdot)$  denotes the proposed SnowFormer network,  $I(x)$  is the input snowy image, and  $Y$  is the corresponding ground truth image.

To further enhance the perceptual quality of the restored images, we also incorporate a perceptual loss. This loss is computed on feature maps extracted from specified layers of a pretrained VGG-19 network and is formulated as:

$$L_{\text{perceptual}} = \sum_{j=1}^2 \frac{1}{C_j H_j W_j} \|\phi_j(S(I(x))) - \phi_j(Y)\|_1, \quad (6)$$

where  $\phi_j$  represents the activation of the  $j$ -th selected layer in VGG-19, and  $C_j$ ,  $H_j$ , and  $W_j$  correspond to the number of channels, height, and width of the feature map at that layer, respectively.

The overall loss function is expressed as a weighted sum of the reconstruction and perceptual losses:

$$L = \lambda_1 L_{L1} + \lambda_2 L_{\text{perceptual}}, \quad (7)$$

where  $\lambda_1$  and  $\lambda_2$  are empirically set to 1 and 0.2, respectively.

## V. IMPLEMENTATION DETAILS

We implement our method using PyTorch [41] on a single NVIDIA RTX 4090 GPU. During training, we use a batch size of 4 and a learning rate of  $10^{-4}$  with the Adam optimizer [42]. The images and events are cropped and resized to  $256 \times 256$ . The events are accumulated over 10 ms and converted to a voxel-grid representation with 10 channels.

## VI. EVALUATION

We now describe the evaluation of our proposed method on the DSEC-Snow dataset and the real snow dataset. We compare our method with existing state-of-the-art methods for the task of snow occlusion removal. We also perform ablation studies to understand the effect of events and images on the performance of our method. Our method is evaluated using the following metrics:

- Peak Signal-to-Noise Ratio (PSNR): Higher PSNR indicates better quality of the reconstructed image.
- Structural Similarity Index (SSIM): Higher SSIM indicates greater similarity between the reconstructed image and the ground-truth image.

In addition, we evaluate the performance of our method on downstream tasks such as object detection, depth estimation, and optical flow using their corresponding standard metrics.

**Baselines** We consider state-of-the-art single-image de-snowing approaches proposed in [1], [2]. In addition, we consider the RLP model proposed in [20], which introduces a novel method for night-time deraining. This is specifically considered as the rain in the night-time sequences has a similar appearance to snow occlusions. We also consider the state-of-the-art publicly available video-based de-snowing approach S2VD [35]. Additionally, we include the E2VID [43] method, for event-based image reconstruction method.

## VII. DATASET

To the best of our knowledge, there exists no dataset consisting of events for de-snowing. Moreover, obtaining accurate ground-truth for such a task is also quite challenging. Previous image-based and video-based approaches relied on simulated datasets such as SnowCity [5], SnowKITTI [5] to train and evaluate their models. However, due to the limited framerate of the cameras, simulating events from these videos is not possible. We therefore propose to use real events recorded by a physical event camera for both the snow and background movement. Our dataset uses a popular visual effect technique called ‘‘Chroma key compositing’’. We record two independent sequences consisting of background motion and foreground motion using a real event camera and RGB camera. The foreground motion is recorded in front of a black screen to have maximum contrast between the snow particles and the background. These events are then overlaid on the background events as described in Section VII. To show the performance of our approach with real snowfall, we also record driving sequences in snowfall using a real event camera. We describe this in detail in Section VII-B.

### A. DSEC-Snowdataset

Accurate simulation of image degradation due to weather conditions has been a popular research topic as it provides a supervision signal in the form of ground-truth clean images, the ability to generate large-scale datasets, and a benchmark to evaluate methods. Generating synthetic snow-occluded images and video has been proposed in the past [5], [8], which overlay realistic snow occlusions on top of clean images, providing

---

**Algorithm 2** Synthetic event stream generation using real background and snow occlusion events.

---

*Input:* Clean background image  $J(x)$ , background events  $E_{\text{haze}}(x)$ , snow events  $E_{\text{snow}}(x)$ , haze parameters ( $A$ ).

*Output:* Snow-occluded image  $Z(x)$ , synthetic events  $E(x)$ .

*Procedure:*

Compute depth map  $D(x)$  from  $J(x)$  using a depth estimation model [45].

Generate haze image  $I_{\text{haze}}(x)$  using  $D(x)$  and atmospheric scattering model [46].

Overlay snow events on  $I_{\text{haze}}(x)$  to obtain  $Z(x)$ .

Initialize synthetic event stream  $E(x) \leftarrow \emptyset$

For each event  $e_{\text{snow}} \in E_{\text{snow}}(x)$ :

Given event location  $(x, y)$  and timestamp  $t$

If  $|I_{\text{haze}}(x, y) - I_{\text{snow}}(x, y)| > C$ , add  $e_{\text{snow}}$  to  $E(x)$

For each event  $e_{\text{haze}} \in E_{\text{haze}}(x)$ :

Given event location  $(x, y)$  and timestamp  $t$

If there is no overlapping  $e_{\text{snow}}$  at  $(x, y, t)$  in  $E(x)$ , add  $e_{\text{haze}}$  to  $E(x)$

**return**  $Z(x), E(x)$

---

ground-truth for training and evaluation. We adopt a similar approach for generating the snow-occluded images in our dataset. The clean image ( $J(x)$ ) is taken from the DSEC dataset [16], which consists of driving sequences recorded using a Prophesee event camera and RGB camera mounted on a car while driving in different cities in Switzerland. The snow occlusions are separately recorded using a real event camera during a snowfall. These snow occlusions are overlaid on the background image to produce a snow-occluded image ( $I_{\text{snow}}(x)$ ), similar to the approach used in [8]. To add realistic snow image degradation, we also render haze on the background image based on the atmospheric scattering model [44]:

$$I_{\text{haze}}(x) = J(x) \cdot t(x) + A \cdot (1 - t(x)), \quad (8)$$

where  $t(x)$  is the transmission map,  $A$  is the atmospheric light, and  $J(x)$  is the background image. The transmission map is computed using the depth map of the image computed by [45]. The snow rendering is done by overlaying the snow occlusion on the background image:

$$Z(x) = I_{\text{haze}}(x) + \alpha \cdot \text{Aug}(E_{\text{snow}}(x)), \quad (9)$$

where  $Z(x)$  is the final image,  $\alpha$  models ambient illumination of the scene [8], and  $\text{Aug}(E_{\text{snow}}(x))$  is the augmentation function that simulates the occluded image from foreground snow events.

While such realistic rendering of snow occlusion is possible for images, for events, generating events that simulate the real world and the real sensor is quite challenging and still an open problem [47]. We therefore propose to instead use a unique method to generate a synthetic dataset by combining multiple

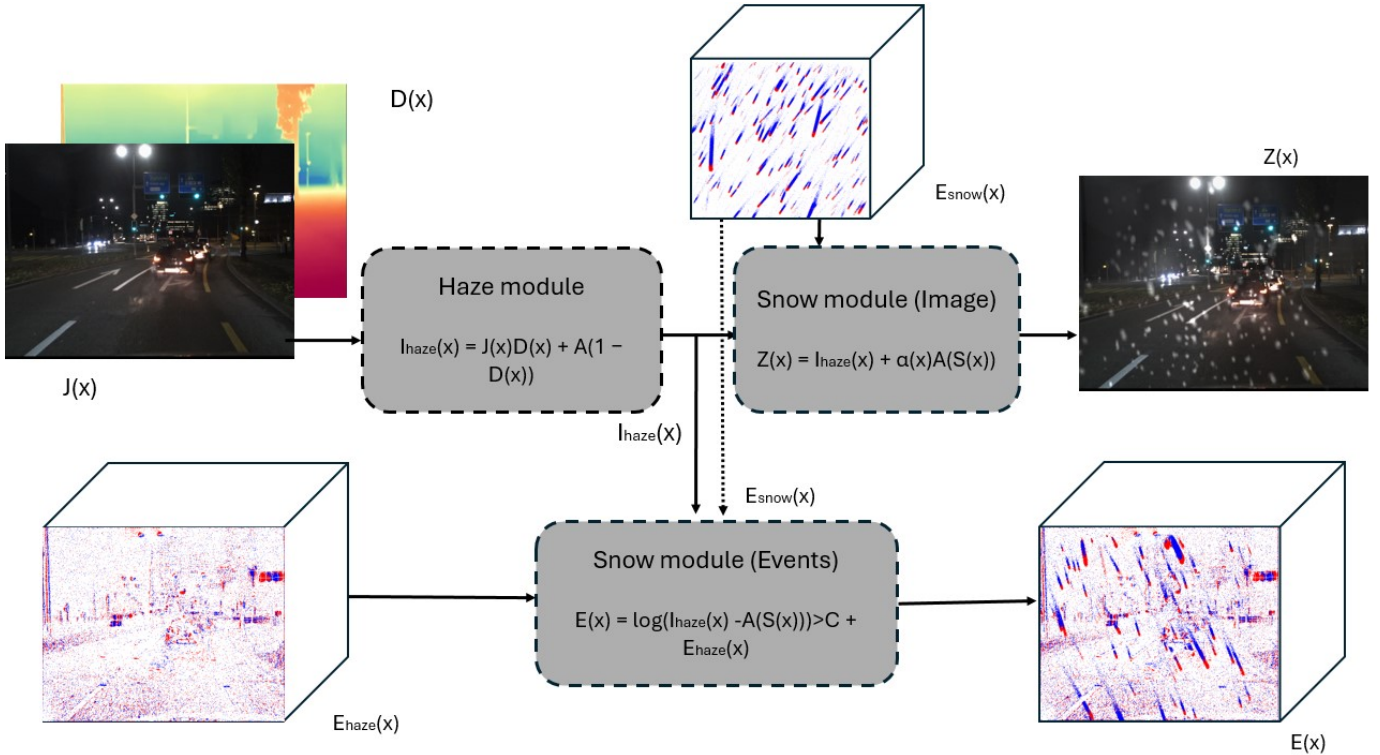


Fig. 4: **Overview of the synthetic snow dataset generation process.** Given a clean background image  $J(x)$  and its corresponding event stream  $E_{haze}(x)$  and foreground snow event stream  $E_{snow}(x)$ , we generate a synthetic snow-occluded image  $Z(x)$  and a synthetic event stream  $E(x)$ . The haze module generates a hazy image  $I_{haze}(x)$  using an atmospheric scattering model [44] based on the background image  $J(x)$  and its depth map. The snow module overlays snow onto the hazy image to produce the snow-occluded image  $Z(x)$ . Simultaneously, background events  $E_{haze}(x)$  and snow events  $E_{snow}(x)$  are combined to generate the final event stream  $E(x)$ .

event streams recorded with a real event camera, as shown in Fig. 4. It consists of recording two event streams, one corresponding to background motion resulting from camera movement ( $E_{haze}$ ) and a second event stream corresponding to the motion of occlusion such as snow ( $E_{snow}$ ). These events are combined using the process described below.

Incorporating the “chroma key compositing” technique, we record the snow particles in front of a black screen. These foreground events are merged with the background events using two main criteria:

- Background intensity correction: Events are only generated if there exists a contrast between the snowflake ( $I_{snow}$ ) and the background. Since snowflakes are typically bright [9], brighter backgrounds will not generate events even if a snowflake moves across a bright pixel.
- Background events overlap: In the case where background activity generates events at the same time as the occlusion, priority is given to the occlusion event as the occlusion is typically in front of the scene.

The algorithm described above is also summarized in 2

Some examples from these sequences are shown in Fig. 6. More details about our dataset can be found in the supplementary material.

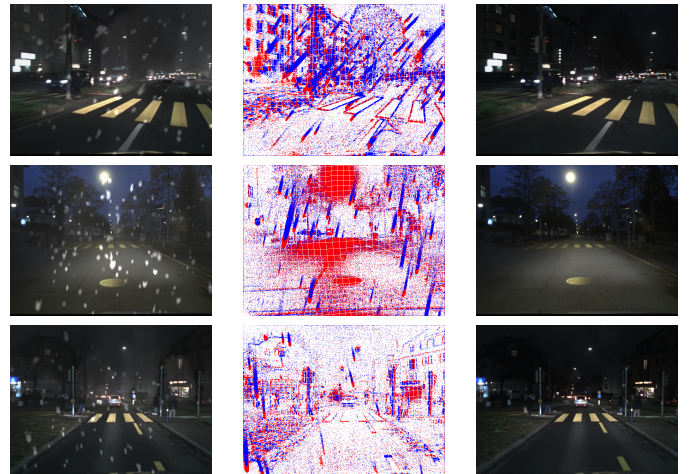


Fig. 5: **Example scenes from our DSEC-Snowdataset.** It consists of synchronized RGB frames(Left), Events (Middle) and Groundtruth (Right).

### B. Slider-Snowdataset

To evaluate the model on real data, we propose to collect our own dataset. Evaluating with real snowfall, however, is quite challenging as there is no ground-truth available. We therefore

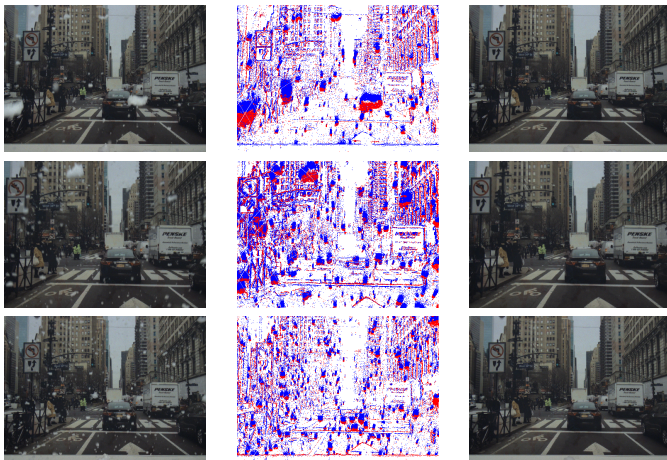


Fig. 6: **Examples scenes from our Slider-Snowdataset** It consists of synchronized RGB frames(Left), Events (Middle) and Groundtruth (Right).

propose to use a controlled setup to evaluate the performance in the real world, using a snow machine. We use a linear slider to move the event camera at a fixed velocity while recording the snowfall using a snow machine. This allows us to record sequences with snowfall and ground-truth data. The details about the setup and data generation process are shown in Fig. 7 and elaborated in the supplementary material.



Fig. 7: **Overview of the experimental setups** (a) Our setup for recording the foreground occlusion events used for generating DSEC-Snowsequence. (b) Experimental setup for our controlled real-world dataset. The scene was printed on a poster and the camera was placed on a linear slider with a fixed velocity and acceleration. The snowfall was simulated using a snow machine.

### C. Real Snowfall Driving Sequences

Finally, we also collect a new dataset consisting of real snowfall driving sequences. We use the BeamSplitter setup of the Prophesee event camera [48] and FLIR BlackFly S global shutter RGB camera mounted on the dashboard of the car while driving in the snowfall. Of course, as there is no ground-truth available, we only use these sequences for qualitative evaluation. Some examples from these sequences are shown in Fig. 6. For evaluating our method on real-world driving datasets, we finetune our model on the night sequences of DSEC-Snowdataset.

Method	Input	DSEC-Snow		Slider-Snow	
		PSNR	SSIM	PSNR	SSIM
Restormer [1]	I	20.37	0.7031	25.16	0.8939
SnowFormer [2]	I	21.48	0.7294	17.63	0.5593
RLP [20]	I	11.26	0.4882	10.10	0.6062
S2VD [35]	V	20.67	0.7204	25.16	0.8706
E2VID [43]	E	11.94	0.4280	15.77	0.3416
Model-based	E+I	20.80	0.6372	19.81	0.6254
Ours	E + I	<b>28.08</b>	<b>0.8621</b>	<b>21.55</b>	<b>0.6832</b>

TABLE II: **Quantitative comparison of image desnowing methods on our DSEC-Snow and Slider-Snow datasets** We report PSNR and SSIM for each method using different input modalities: intensity images (I), video (V), events (E), and both (E+I). The proposed approach, leveraging both event and image data, demonstrates higher image reconstruction quality compared to existing image-based and event-based methods.

## VIII. RESULTS

We evaluate our method on the DSEC-Snow dataset and the real snow dataset, and compare it with existing state-of-the-art methods in Section VIII-A. We also perform ablation studies to understand the effect of events and images on the performance of our method. In addition, we evaluate the performance of our method on downstream tasks such as object detection, depth estimation, and optical flow using their corresponding standard metrics.

### A. DSEC-SnowDataset

Table II presents a quantitative comparison of various image desnowing methods evaluated on the DSEC-Snow and Slider-Snow datasets, reporting PSNR and SSIM for each method. The image-based approaches (Restormer, SnowFormer, and RLP) which rely solely on intensity images (I) show moderate performance. Since RLP was trained for night-time deraining, it struggled to generalize to day-time occlusions which is evident from the low PSNR and SSIM scores. Video-based methods (S2VD) leverage temporal information from video sequences, achieving better results than single-image methods, but still fall short of the performance of our proposed method, as events provide high resolution temporal information that videos of 20 fps cannot capture. Notably, event-only methods (E2VID) perform significantly worse, particularly in terms of SSIM, indicating that events alone are insufficient for effective desnowing in highly occluded scenes. Model-based fusion of events and images (E+I) shows improved PSNR over single-modality approaches; however, the overall image quality is low (indicated by low SSIM scores), suggesting that naive fusion of modalities does not capture the complex spatio-temporal patterns of snow occlusions effectively. In comparison to all, our method, which fuses both event and intensity information (E+I), achieves the highest PSNR and SSIM across both datasets, outperforming all baselines by a significant margin. Qualitative results are shown in Fig. 9, where our method effectively removes snow occlusions while preserving fine details of the background scene.

### Ablation on occlusion density

We study the robustness of desnowing methods under varying occlusion conditions in Fig. 10. Each row in the figure

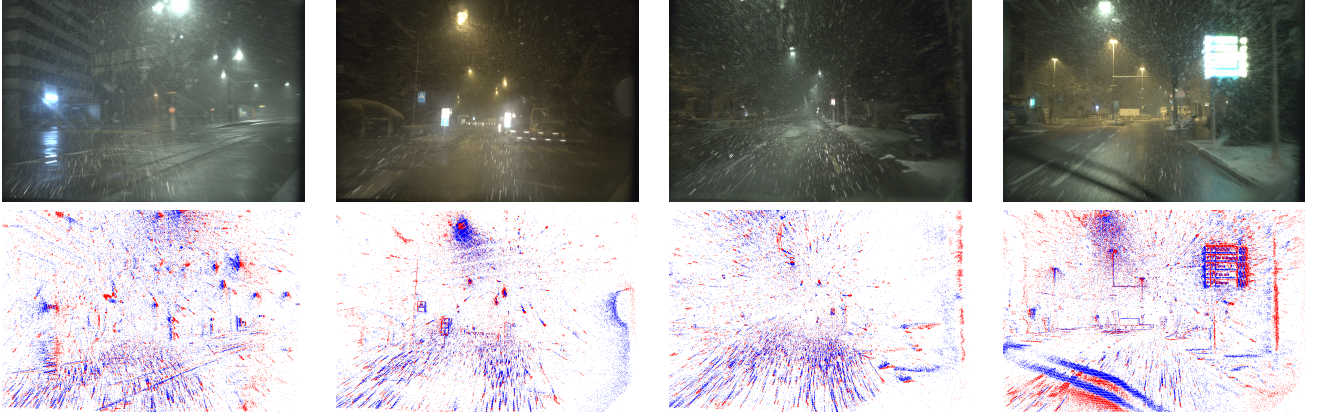


Fig. 8: **Samples from our real-world snowfall driving sequences** The images are recorded using the synchronized and aligned setup of RGB camera (top) and event camera (bottom) and mounted on the dashboard of the car while driving in the snowfall.

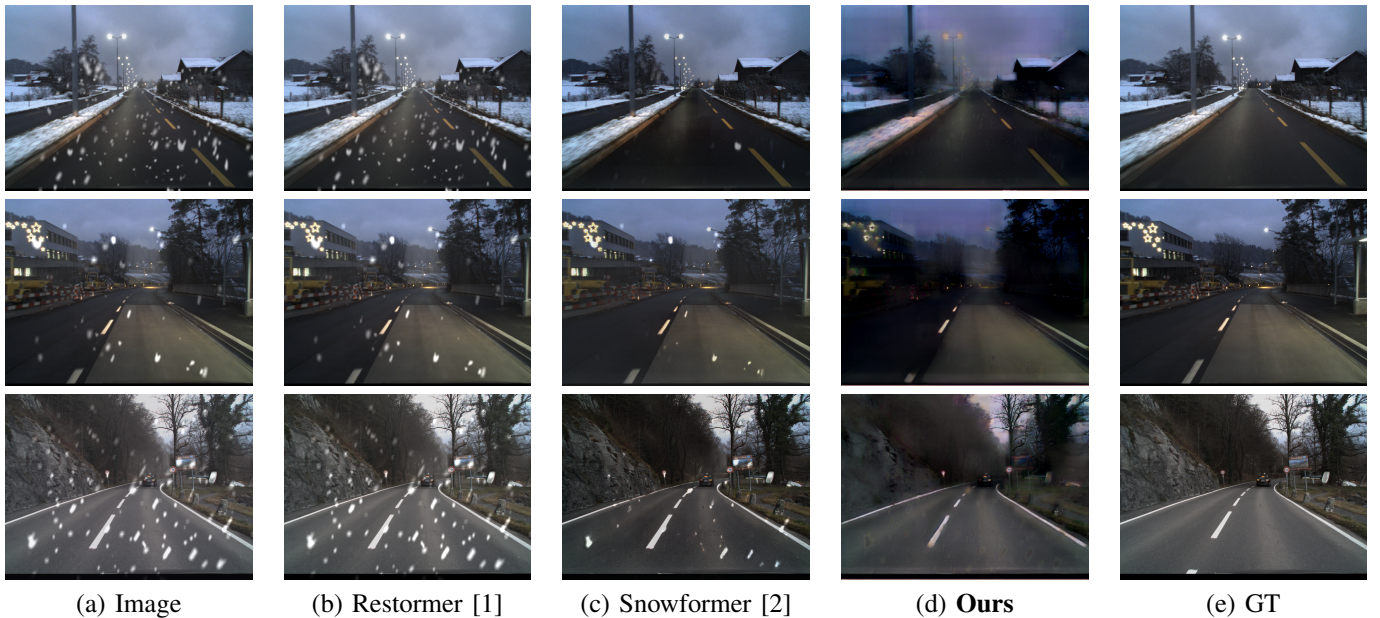


Fig. 9: **Qualitative comparison of image desnowing results on synthetic data.** (a) Input images with synthetic snow, (b)-(c) image restoration baselines, (d) our result, and (e) ground truth (GT) images. The proposed approach recovers clearer scene structures and more faithfully restores the underlying content compared to prior methods.

represents a distinct occlusion density, increasing from top to bottom. As the occlusion density increases, we observe a substantial degradation in scene visibility and reconstruction quality for the image-only and event-only baselines. SnowFormer and RLP exhibit noticeable artifacts and loss of detail under severe occlusions, leaving substantial snow artifacts in the reconstructed outputs. In contrast, our method demonstrates consistent robustness across all occlusion densities, effectively removing snow particles and preserving fine scene details. These results highlight the benefit of jointly leveraging event and image data, enabling our approach to maintain high-quality reconstructions even in highly adverse weather conditions with dense occlusions.

**Effect on downstream application** We also evaluate the performance of our method on the downstream task of optical

flow. We show that our method is able to reconstruct the background scene with high accuracy, resulting in significant improvement in downstream applications, see Fig. 11. We use the RAFT network [49] on the images reconstructed by all image restoration methods and compare the end-point-error (EPE) metric to evaluate the performance of optical flow.

Table III reports the End-Point Error (EPE) and accuracy metrics ( $AE < 1$ ,  $AE < 3$ ,  $AE < 5$ ) for optical flow computed on the Slider-Snowdataset. Event-only (E2VID) and video-based (S2VD) baselines exhibit high EPE and low accuracy, reflecting their limited ability to recover motion information in the presence of severe occlusions. Image-based methods (Restormer, SnowFormer, RLP) provide improved performance, but still suffer from significant error, particularly under challenging conditions. Our approach, which fuses

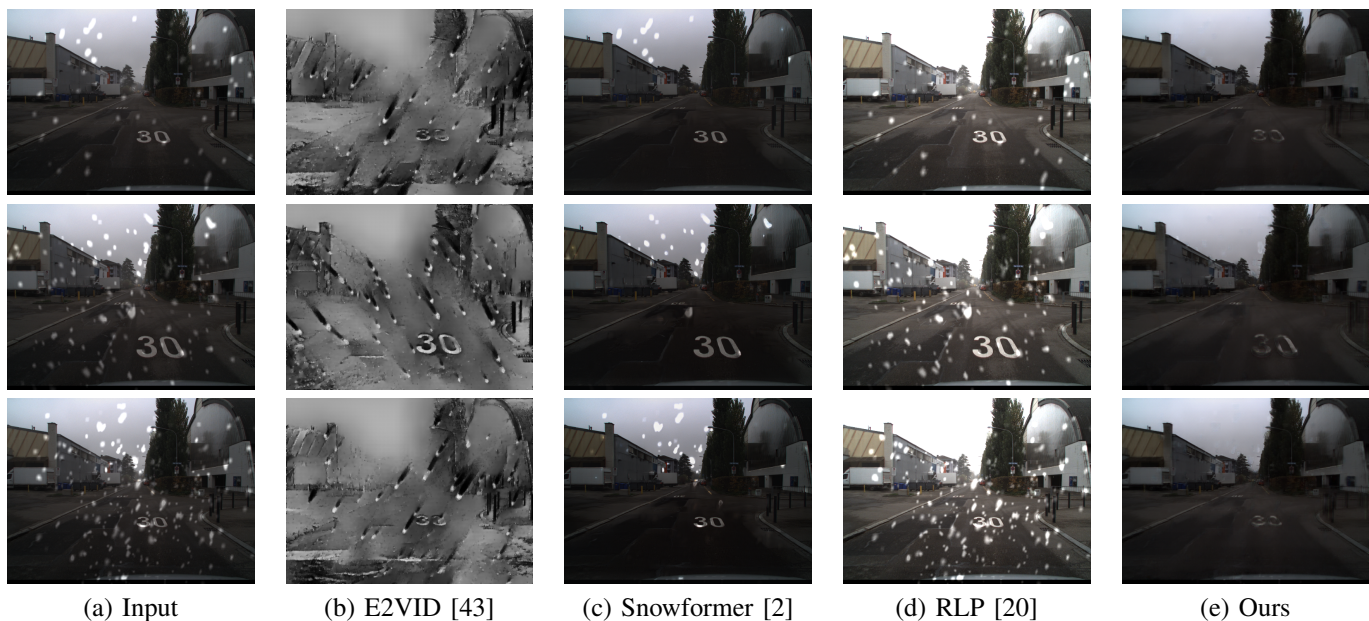


Fig. 10: **Effect of occlusion density on image reconstruction quality** Each row corresponds to a different level of occlusion density, increasing from top to bottom. As occlusion density increases, visibility of scene details and robustness of the image-only algorithm degrade significantly. Our method performs consistently well across all occlusion densities, effectively removing snow occlusions and preserving scene details.

event and intensity modalities, achieves the lowest EPE. The qualitative results in Fig. 11 further confirm these findings: optical flow maps generated using our method are visually closer to the ground truth, accurately capturing fine motion boundaries and overall scene structure, while baseline methods display artifacts and loss of detail. These results indicate that our event-image fusion approach not only improves desnowing quality, but also leads to substantial gains in the downstream tasks such as optical flow estimation.

Method	Input	Optical Flow			
		EPE ↓	$AE < 1 \uparrow$	$AE < 3 \uparrow$	$AE < 5 \uparrow$
Restormer [1]	I	31.43	<b>0.025</b>	<b>0.284</b>	0.412
SnowFormer [2]	I	30.65	0.015	0.210	0.350
RLP [20]	I	27.33	0.023	0.273	<b>0.421</b>
S2VD [2]	V	42.16	0.018	0.217	0.327
E2VID [43]	E	90.83	0.001	0.011	0.029
Ours (Model-based)	E+I	30.72	0.009	0.158	0.290
Ours	E+I	<b>22.64</b>	0.007	0.130	0.270

TABLE III: **Quantitative evaluation of downstream task (optical flow)**—on desnowed images using different restoration methods and input modalities. Our event-image fusion approach consistently achieves the best performance across all tasks, as measured by EPE and accuracy for optical flow.

### B. Results on Slider-SnowDataset

We further evaluate our method on a real-world snowfall dataset to assess its generalization ability beyond the synthetic domain. Specifically, we deploy the model trained on our synthetic DSEC-Snow dataset and apply it directly to the Slider-Snowdataset, which is captured under real snowfall conditions. Figure 12 compares our method to both a degraded input image and a strong image-based baseline, Restormer [1].

In all rows, our approach (column d) consistently produces better reconstructions compared to both the original occluded image (column a) and Restormer (column b). Notably, in the first and third rows, where dense snowflakes heavily obscure vehicle details, our method is able to restore the underlying vehicle contours and even fine-grained elements such as traffic signs, which are either blurred or completely lost in the baseline. In the second row, our reconstruction restores facade textures and depth boundaries that are completely wiped out in the Restormer output due to heavy occlusion. Additionally, in the fourth row, where snow occludes building structures with fine geometry, our method is able to infer and reconstruct the linear architectural details more faithfully.

These qualitative improvements highlight the strength of using event data for temporally consistent, occlusion-aware image reconstruction. By attending to motion patterns in the event stream, our model infers occluded content more robustly than purely image-based approaches. Importantly, the model is not fine-tuned on real-world snow data, indicating strong cross-domain generalization. This result validates the effectiveness of our synthetic dataset generation pipeline and supports its applicability for training models deployable in real-world conditions. Qualitative results are shown in Fig. 12.

### C. Results on real snowfall driving sequences

We also evaluate our method on real-world snowfall driving sequences acquired using a beamsplitter-based sensor rig comprising a Prophesee Gen4 event camera (1280×720) and a FLIR BlackFly S global shutter RGB camera (1440×1080). This setup enables temporally aligned acquisition of high-dynamic-range (HDR) event data and intensity frames under

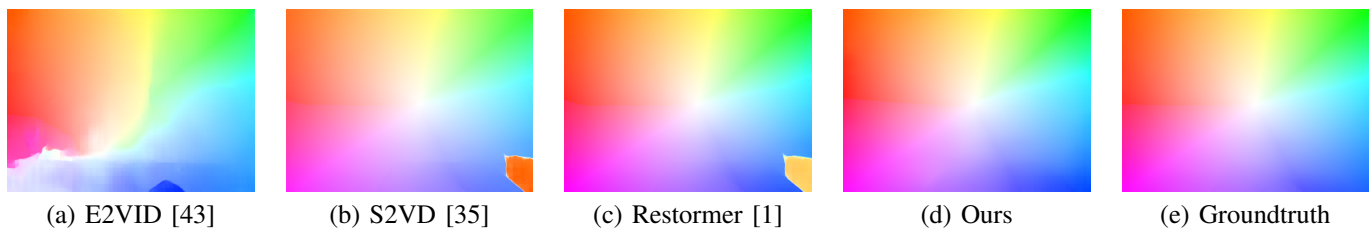


Fig. 11: **Comparing the image reconstruction, optical flow estimation** for event-only baseline E2VID, video baseline S2VD, and image baseline Restormer with our method on the Slider-Snowdataset.

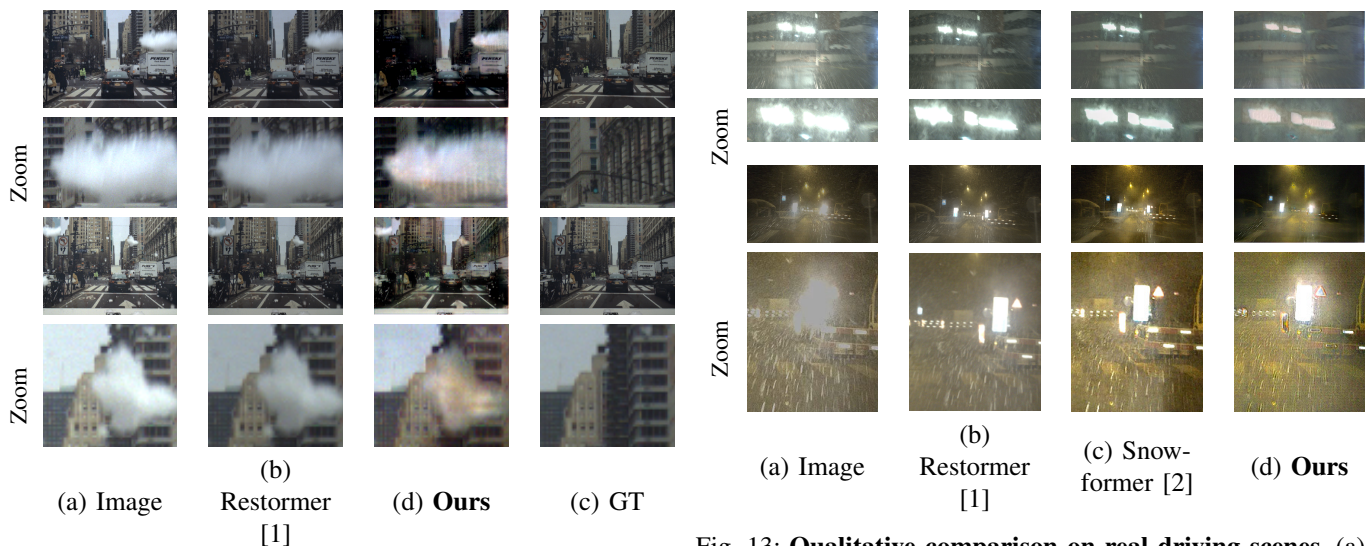


Fig. 12: **Qualitative comparison on Slider-Snowdataset** The first row shows the original images, restoration results from Restormer [1], our method, and the ground truth (GT) images. The second row presents zoomed-in views of challenging occluded regions, highlighting the improved snow removal and detail recovery (such as the building behind the snowflake) achieved by our approach compared to prior methods.

challenging low-light and high-motion conditions. Qualitative results are presented in Fig. 13.

Our method demonstrates a clear advantage in removing snow-induced occlusions and recovering underlying scene structure. The baseline RGB-only methods, Restormer [1] and Snowformer [2], struggle with motion blur and fail to distinguish snowflakes from meaningful scene content, often resulting in over-smoothed or distorted reconstructions. In contrast, our method preserves high-frequency details and recovers semantically relevant features such as traffic signs, barriers, and road markings, even under heavy snowfall.

The zoomed-in crops in the second and fourth rows of Fig. 13 illustrate this further. In the first sequence, both Restormer and Snowformer fail to recover the text on illuminated signs, which appear severely blurred or overexposed due to specular reflections. Our method, by integrating event-based temporal contrast, is able to suppress the transient occlusions and reconstruct the signage with significantly higher fidelity.

In the second sequence, where oncoming headlights and snowflakes dominate the visual field, the image-only base-

lines suffer from halo artifacts and flare-induced saturation. Our approach effectively suppresses such artifacts, allowing visibility of distant road features, including lane markers and background vehicles. This is largely attributable to the asynchronous, high-temporal-resolution nature of the event data, which captures scene dynamics without the integration-based blur inherent to conventional RGB sensors.

Furthermore, the HDR capability of the event camera plays a crucial role in preserving scene content that is otherwise obscured by strong light sources or wet surfaces on the windshield. Even in scenarios with intense flare or extreme contrast between dark and bright regions, our fusion method maintains consistent reconstruction quality and scene coherence.

The qualitative comparisons in Fig. 13 validate the effectiveness of our approach in real-world adverse weather conditions. By leveraging the complementary sensing modalities of events and images, our method achieves robust occlusion removal and scene restoration beyond the capability of state-of-the-art RGB-only models. More results are available in the supplementary material.

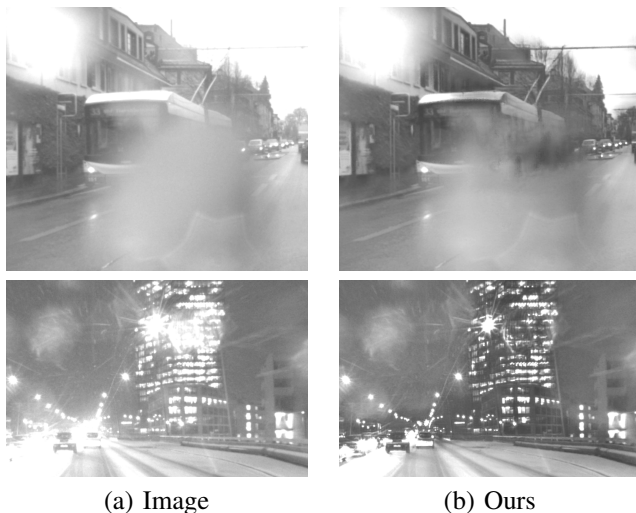


Fig. 14: **Qualitative comparison on the MUSES Dataset [50] with rain and snow occlusions.** (a) Input images affected by rain or snow occlusions, and (b) results from our method. The examples show the effectiveness of our approach in handling adverse weather occlusions across different datasets.

#### D. Generalization to other occlusions

We also consider the all-weather driving dataset proposed in [50], which contains synchronized and calibrated events, images, LiDAR, and RADAR measurements. We only consider the sequences which have a mix of snow and rainfall. Unfortunately, the snowfall is not dense enough in these sequences to hinder the view, unlike our dataset which was collected in heavy snowfall. Nevertheless, we show the qualitative evaluation of our approach in Fig. 14. By fusing temporal information from events, we are able to recover the bus in the background of the raindrop and building, which was occluded by a raindrop causing lens flare.

### IX. DISCUSSION AND LIMITATIONS

While our proposed synthetic dataset provides a practical and physically grounded approach to simulating event-based occlusions, it relies on the assumption that independently captured motions—such as background and occluder (e.g., snowflake) events—can be linearly combined without introducing artifacts. This simplification does not account for interdependencies such as lighting interactions, occlusion ordering, or nonlinear sensor responses, which may be present in real-world scenes. Moreover, the compositing process assumes static scene depth during fusion, which could be limiting in highly dynamic or multi-depth environments.

Another inherent limitation arises from the characteristics of event cameras themselves. Events are triggered only when a local brightness change exceeds a sensor-defined contrast threshold (typically around 15%). As a result, regions with flat textures, uniform lighting, or minimal motion fail to produce meaningful event activity. This restricts the utility of our approach in low-texture environments or scenes where fine-grained intensity variations fall below the contrast threshold. Consequently, the reconstruction quality is strongly tied to the

presence of high-frequency spatial and temporal information in the scene.

Despite these limitations, our approach offers a scalable and flexible alternative to traditional physics-based simulators, which often require complex modeling of event camera characteristics. Notably, the dataset generation methodology can be extended beyond weather simulation: any independently recordable motion (e.g., pedestrians, vehicles, or dynamic objects) can be composited over different backgrounds to augment data diversity in a controlled manner. This makes the method valuable for a wide range of applications such as robotics, autonomous driving, and dynamic scene understanding, where controlled yet realistic event-based data are scarce.

### X. CONCLUSION

We introduce a novel event-based approach for background image reconstruction in the presence of dynamic occlusions. It leverages the complementary nature of event cameras and frames to reconstruct true scene information instead of hallucinating occluded areas as done by image inpainting approaches. Specifically, our proposed data-driven approach reconstructs the background image using only one occluded image and events. The high temporal resolution of the events provides our method with additional information on the relative intensity changes between the foreground and background, making it robust to dense occlusions. To evaluate our approach, we present the first large-scale dataset recorded in the real world containing challenging scenes with synchronized events, occluded images, and ground-truth images. Our method achieves an improvement of 3 dB in PSNR over state-of-the-art frame-based and event-based methods on both synthetic and real datasets. We believe that our proposed method and dataset lay the foundation for future research.

## XI. DSEC-SNOWDATASET

We show the setup used here to record the dataset. We give a detailed overview of the data generation process that was used to create DSEC-Snowdataset. We used a black background to maximize the contrast between the foreground and background as shown in experimental setup. The underlying assumption in this setup is that snow particles tend to be brighter than most objects in the surrounding. Therefore to maximize the contrast between every snowflake movement and background, we use a black screen. These events can then be pruned to account for arbitrary background. Second assumption which we make is that snowflakes will always be in the foreground, i.e they will never be occluded by the background, which for most common scenarios is a reasonable assumption. Of-course this also means we do not model any depth perception in this fusion and treat foreground events as far away from background. Lastly, as of now we do not model the motion of the snow particles according to ego-motion of the camera. In typical driving scenarios, the ego-motion of the car makes the snowflake appear coming towards the camera rather than simply flying down. This ofcourse is a function of the speed of the camera and makes this matter of simulating accurate motion of snowflakes quite challenging. We therefore simplify this problem and only apply homography transformation to the foreground events. Overall our dataset consists of around 200 training and 50 test sequences, where each sequence consisting of a short duration of driving with snowfall in both day and night.

**Augmentation Parameters** We describe in detail the augmentation parameters used to generate the dataset. Similar to method proposed in [8], we render different effects of snowfall on the image such as haze and illumination dependent snow appearance. To render haze, we follow the model proposed in [44] which uses the atmospheric scattering model for rendering hazy images. To blend the snow foreground with the background image, we use strategy proposed in [8], by considering the ambient illumination and time of day to blend the snowflakes. For example, during day, snowflakes blend with the sky and are therefore not easily visible with the brighter sky background. This is exactly opposite during the night: snowflakes are more visible in brightly lit areas such as headlamps or streetlight [8]. These hazy images are combined with the foreground snow events to produce the final image. To simulate realistic snow occlusion, we apply different augmentations to the snow events. As describe in Equation. 9, we apply different augmentations to the snow:

- **Snow Speed:** Speed of the snowflakes is artificially controlled by scaling the timestamp of the foreground events.
- **Snow Density:** Density of snowflakes is increased by overlaying multiple snow events by staggering the timestamps and applying homography transformation to the foreground events.
- **Motion Direction:** Motion direction is only controlled by flipping the foreground events along the horizontal axis.

**Simulating Events** The background events correspond to driving sequences recorded using DSEC [16]. It consists of an event camera and RGB camera mounted next to each other

on a car while driving in different cities Switzerland. The background events ( $E_{haze}(x)$ ) are recorded with Prophesee Gen3.1 event camera with a resolution of  $640 \times 480$  pixels. The background images ( $J(x)$ ) are recorded at  $20Hz$  with a resolution of  $1440 \times 1080$  pixels and aligned with the events. Since our approach relies on temporal and spatial alignment of the events and images, we use the rectified and aligned events and images from DSEC dataset.

The foreground events ( $E_{snow}(x)$ ) are recorded using a Prophesee Gen4 event camera with a resolution of  $1280 \times 720$  pixels. The foreground events are recorded in front of black background. It was shown in [51] that signal to noise ratio (SNR) of an event camera depends on illumination and contrast of the scene. As illumination increases, the SNR of the events can drop significantly if the contrast is not high enough. As we were restricted to outdoor recording, we could not control the illumination of the scene, we use a black background to maximize the contrast between the foreground (snow, typically bright) and background, ensuring sufficient SNR when recording the foreground events. Dataset statistics are shown in Fig. 15. The dataset consists of 1000 training and 470 test pairs of images and events. In addition, we provide ground truth images and events for both the training and test sequences. A histogram illustrating the percentage of occluded pixels reveals the distribution of occlusion intensity across the dataset. Most images have occlusion levels concentrated between approximately 13% and 22%, indicating moderate occlusion intensity is prevalent. Fewer instances exhibit extreme occlusion levels, highlighting realistic variability in weather conditions captured by the dataset.

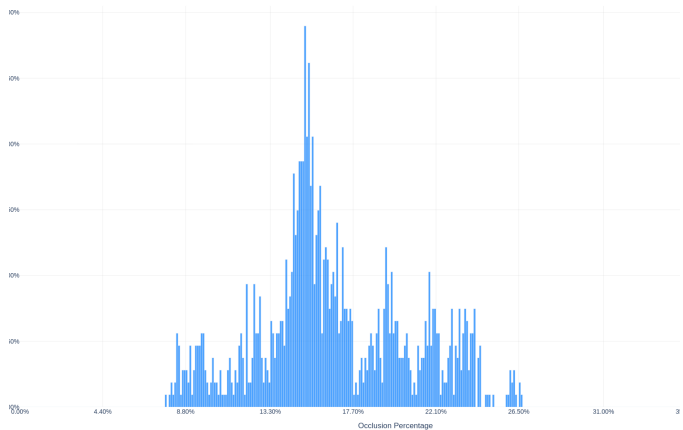


Fig. 15: Dataset statistics of DSEC-Snowdataset. The histogram shows the percentage of occluded pixels in the dataset, illustrating the distribution of occlusion intensity across the dataset.

### A. Comparison with State-of-the-Art Methods

We show samples from our method and compare it with state-of-the-art de-snowing methods on the DSEC-Snowdataset in Fig. 16.

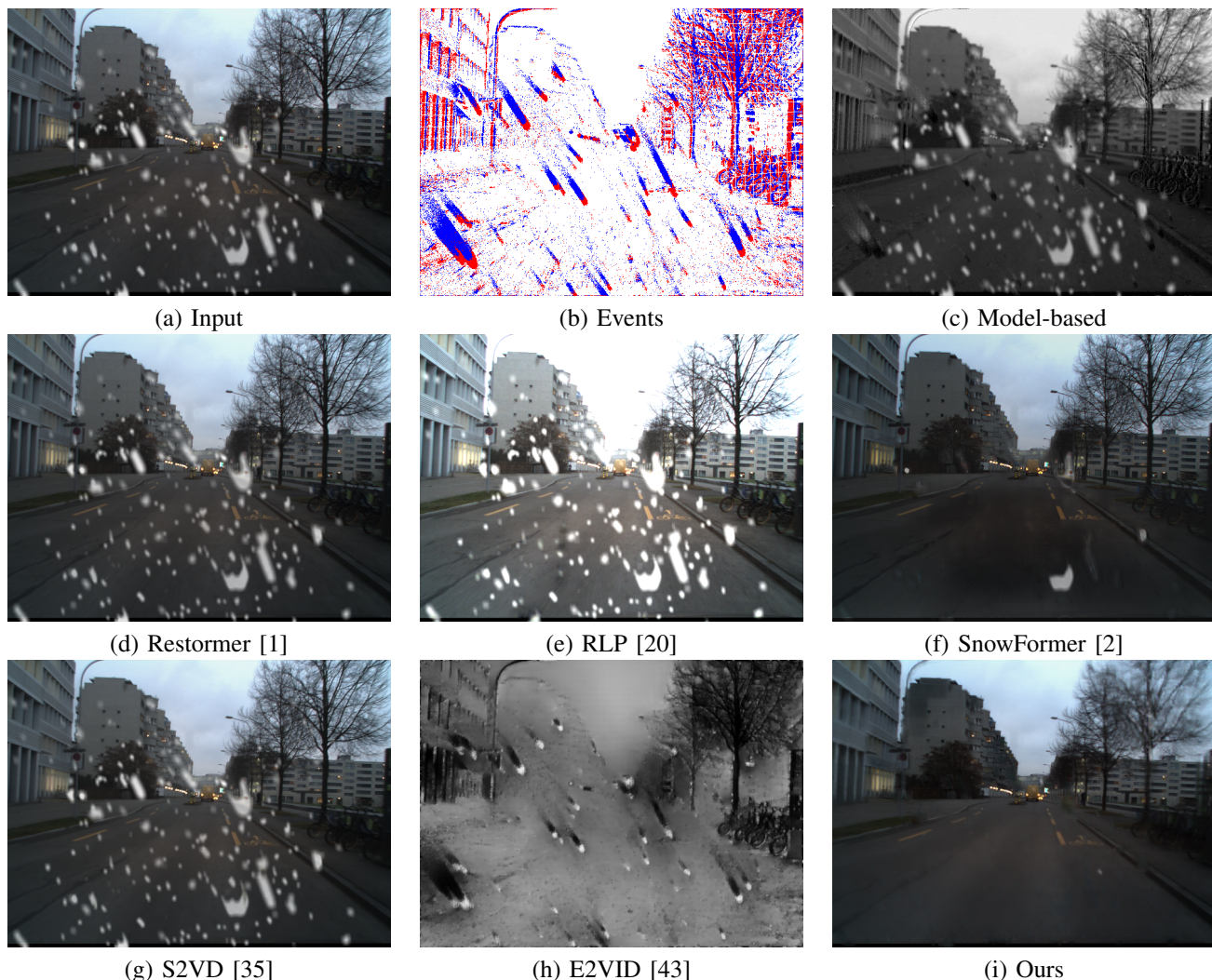


Fig. 16: Comparison of our method with state-of-the-art de-snowing methods on DSEC-Snowdataset.

We show samples from our method and compare it with state-of-the-art de-snowing methods on the Slider-Snowdataset in Fig. 17.

In addition to the qualitative results, we also evaluate our method on a downstream task, depth estimation, using the real driving dataset in Fig. 18.

## XII. ABLATION STUDY ON NETWORK ARCHITECTURE

Model	PSNR (dB)	SSIM	
Naive Fusion	24.92	0.7981	We show an abla-
Ours	28.08	0.8621	

tion study on the network architecture to evaluate the impact of different components on the performance of our method in Table XII. We compare our approach to naive fusion: the events and images are concatenated and provided as input to the transformer backbone. It can be seen that even with a naive fusion approach, we achieve higher PSNR and SSIM than image-only methods. This shows that the events provide useful information for image reconstruction. However, our proposed method outperforms the naive fusion approach by a

significant margin, demonstrating the effectiveness of careful design choices in our architecture.

## REFERENCES

- [1] S. W. Zamir, A. Arora, S. Khan, M. Hayat, F. S. Khan, and M.-H. Yang, “Restormer: Efficient transformer for high-resolution image restoration,” in *CVPR*, 2022.
- [2] S. Chen, T. Ye, Y. Liu, E. Chen, J. Shi, and J. Zhou, “Snowformer: Scale-aware transformer via context interaction for single image desnowing,” *arXiv preprint arXiv:2208.09703*, 2022.
- [3] M. Bijelic, T. Gruber, F. Mannan, F. Kraus, W. Ritter, K. Dietmayer, and F. Heide, “Seeing through fog without seeing fog: Deep multimodal sensor fusion in unseen adverse weather,” in *The IEEE Conference on Computer Vision and Pattern Recognition (CVPR)*, June 2020.
- [4] Y.-F. Liu, D.-W. Jaw, S.-C. Huang, and J.-N. Hwang, “Desnownet: Context-aware deep network for snow removal,” *IEEE Transactions on Image Processing*, vol. 27, no. 6, pp. 3064–3073, 2018.
- [5] K. Zhang, R. Li, Y. Yu, W. Luo, and C. Li, “Deep dense multi-scale network for snow removal using semantic and geometric priors,” *IEEE Transactions on Image Processing*, 2021.
- [6] W.-T. Chen, H.-Y. Fang, J.-J. Ding, C.-C. Tsai, and S.-Y. Kuo, “Jstasr: Joint size and transparency-aware snow removal algorithm based on modified partial convolution and veiling effect removal,” in *European Conference on Computer Vision*, 2020.

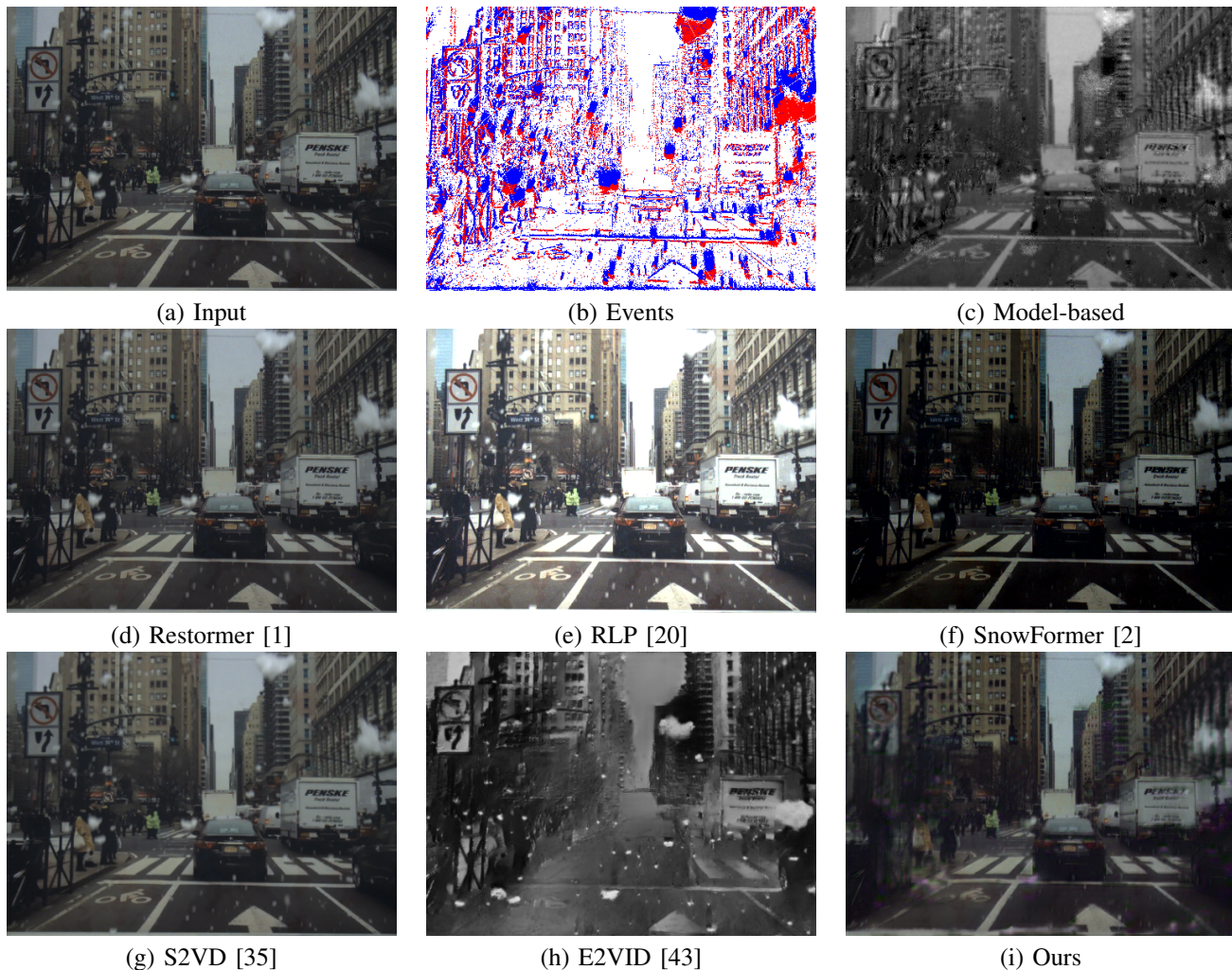


Fig. 17: Comparison of our method with state-of-the-art de-snowing methods on Slider-Snowdataset.

- [7] W.-T. Chen, H.-Y. Fang, C.-L. Hsieh, C.-C. Tsai, I. Chen, J.-J. Ding, S.-Y. Kuo *et al.*, “All snow removed: Single image desnowing algorithm using hierarchical dual-tree complex wavelet representation and contradict channel loss,” in *Proceedings of the IEEE/CVF International Conference on Computer Vision*, 2021, pp. 4196–4205.
- [8] H. Chen, J. Ren, J. Gu, H. Wu, X. Lu, H. Cai, and L. Zhu, “Snow removal in video: A new dataset and a novel method,” in *Proceedings of the IEEE/CVF International Conference on Computer Vision (ICCV)*, October 2023, pp. 13 211–13 222.
- [9] K. Garg and S. Nayar, “When does a camera see rain?” in *Tenth IEEE International Conference on Computer Vision (ICCV’05) Volume 1*, vol. 2, 2005, pp. 1067–1074 Vol. 2.
- [10] B. Yang, Z. Jia, J. Yang, and N. K. Kasabov, “Video snow removal based on self-adaptation snow detection and patch-based gaussian mixture model,” *IEEE Access*, vol. 8, pp. 160 188–160 201, 2020.
- [11] W. Ren, J. Tian, Z. Han, A. Chan, and Y. Tang, “Video desnowing and deraining based on matrix decomposition,” in *2017 IEEE Conference on Computer Vision and Pattern Recognition (CVPR)*, 2017, pp. 2838–2847.
- [12] M. Li, X. Cao, Q. Zhao, L. Zhang, and D. Meng, “Online rain/snow removal from surveillance videos,” *IEEE Transactions on Image Processing*, vol. 30, pp. 2029–2044, 2021.
- [13] M. Li, X. Cao, Q. Zhao, L. Zhang, C. Gao, and D. Meng, “Video rain/snow removal by transformed online multiscale convolutional sparse coding,” *ArXiv*, vol. abs/1909.06148, 2019. [Online]. Available: <https://api.semanticscholar.org/CorpusID:202572625>
- [14] J.-H. Kim, J.-Y. Sim, and C.-S. Kim, “Video deraining and desnowing using temporal correlation and low-rank matrix completion,” *IEEE Transactions on Image Processing*, vol. 24, no. 9, pp. 2658–2670, 2015.
- [15] G. Gallego, T. Delbruck, G. Orchard, C. Bartolozzi, B. Taba, A. Censi, S. Leutenegger, A. Davison, J. Conradt, K. Daniilidis, and D. Scaramuzza, “Event-based vision: A survey,” *IEEE Trans. Pattern Anal. Mach. Intell.*, 2020.
- [16] M. Gehrig, W. Aarents, D. Gehrig, and D. Scaramuzza, “Dsec: A stereo event camera dataset for driving scenarios,” *IEEE Robot. Autom. Lett.*, 2021.
- [17] K. Garg and S. Nayar, “Detection and removal of rain from videos,” in *Proceedings of the 2004 IEEE Computer Society Conference on Computer Vision and Pattern Recognition, 2004. CVPR 2004.*, vol. 1, 2004, pp. I–I.
- [18] L.-W. Kang, C.-W. Lin, and Y.-H. Fu, “Automatic single-image-based rain streaks removal via image decomposition,” *IEEE Transactions on Image Processing*, vol. 21, no. 4, pp. 1742–1755, 2012.
- [19] W. Yang, R. T. Tan, S. Wang, Y. Fang, and J. Liu, “Single image deraining: From model-based to data-driven and beyond,” vol. 43, no. 11, 2021, pp. 4059–4077.
- [20] F. Zhang, S. You, Y. Li, and Y. Fu, “Learning rain location prior for nighttime deraining,” in *Proceedings of the IEEE/CVF International Conference on Computer Vision (ICCV)*, October 2023, pp. 13 148–13 157.
- [21] P. Liu, J. Xu, J. Liu, and X. Tang, “Pixel based temporal analysis using chromatic property for removing rain from videos,” *Computer and Information Science*, vol. 2, no. 1, pp. 53–60, 2009.
- [22] X. Zhang, H. Li, Y. Qi, W. K. Leow, and T. K. Ng, “Rain removal in video by combining temporal and chromatic properties,” in *Proceedings of the IEEE International Conference on Multimedia and Expo (ICME)*, 2006, pp. 461–464.
- [23] P. C. Barnum, S. Narasimhan, and T. Kanade, “Analysis of rain and

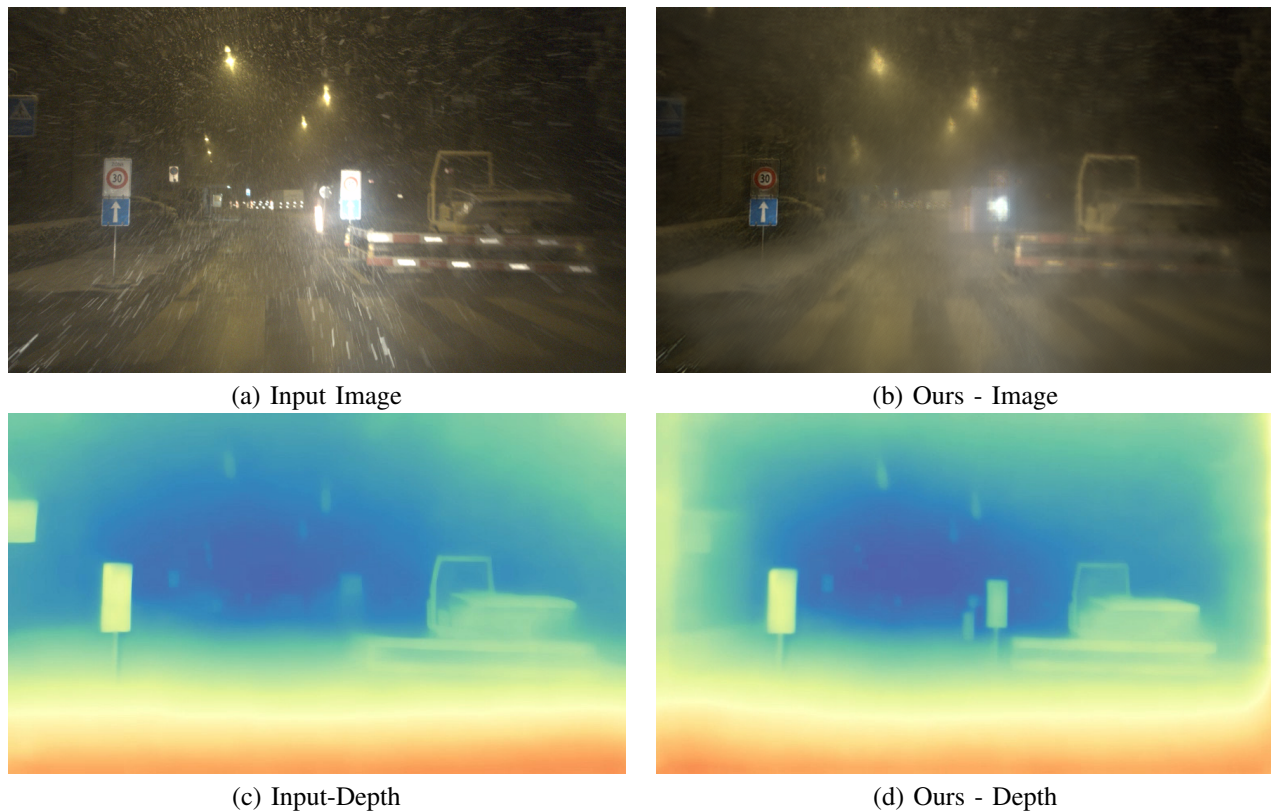


Fig. 18: **Qualitative results of our method on downstream task - depth estimation.** We show the input image and depth map from the DSEC-Snow dataset, along with the depth map generated by our method. The depth map is estimated using the input image and events, demonstrating the effectiveness of our approach in leveraging both modalities for improved depth estimation in snowy conditions.

- snow in frequency space,” *International Journal of Computer Vision*, vol. 86, no. 2-3, p. 256, 2010.
- [24] J. Bossu, N. Hautière, and J.-P. Tarel, “Rain or snow detection in image sequences through use of a histogram of orientation of streaks,” *International Journal of Computer Vision*, vol. 93, no. 3, pp. 348–367, 2011.
- [25] V. Santhaseelan and V. K. Asari, “Utilizing local phase information to remove rain from video,” *International Journal of Computer Vision*, vol. 112, no. 1, pp. 71–89, 2015.
- [26] Y.-L. Chen and C.-T. Hsu, “A generalized low-rank appearance model for spatio-temporally correlated rain streaks,” in *Proceedings of the IEEE International Conference on Computer Vision (ICCV)*, 2013, pp. 1968–1975.
- [27] T.-X. Jiang, T.-Z. Huang, X.-L. Zhao, L.-J. Deng, and Y. Wang, “A novel tensor-based video rain streaks removal approach via utilizing discriminatively intrinsic priors,” in *Proceedings of the IEEE Conference on Computer Vision and Pattern Recognition (CVPR)*, 2017, pp. 2818–2827.
- [28] W. Ren, J. Tian, Z. Han, A. Chan, and Y. Tang, “Video desnowing and deraining based on matrix decomposition,” in *Proceedings of the IEEE Conference on Computer Vision and Pattern Recognition (CVPR)*, 2017, pp. 4210–4219.
- [29] M. Li, Q. Xie, Q. Zhao, W. Wei, S. Gu, J. Tao, and D. Meng, “Video rain streak removal by multiscale convolutional sparse coding,” in *Proceedings of the IEEE Conference on Computer Vision and Pattern Recognition (CVPR)*, 2018, pp. 6644–6653.
- [30] J. Chen, C.-H. Tan, J. Hou, L.-P. Chau, and H. Li, “Robust video content alignment and compensation for rain removal in a cnn framework,” in *Proceedings of the IEEE Conference on Computer Vision and Pattern Recognition (CVPR)*, 2018, pp. 6286–6295.
- [31] J. Liu, W. Yang, S. Yang, and Z. Guo, “Erase or fill? deep joint recurrent rain removal and reconstruction in videos,” in *Proceedings of the IEEE Conference on Computer Vision and Pattern Recognition (CVPR)*, 2018, pp. 3233–3242.
- [32] —, “D3r-net: Dynamic routing residue recurrent network for video rain removal,” *IEEE Transactions on Image Processing*, vol. 28, no. 2, pp. 699–712, 2018.
- [33] W. Yang, J. Liu, and J. Feng, “Frame-consistent recurrent video deraining with dual-level flow,” in *Proceedings of the IEEE Conference on Computer Vision and Pattern Recognition (CVPR)*, 2019, pp. 1661–1670.
- [34] H. Jin, P. Favaro, and S. Soatto, “A semi-direct approach to structure from motion,” *The Visual Computer*, vol. 19, no. 6, pp. 377–394, 2003.
- [35] Z. Yue, J. Xie, Q. Zhao, and D. Meng, “Semi-supervised video deraining with dynamical rain generator,” in *Proceedings of the IEEE/CVF Conference on Computer Vision and Pattern Recognition*, 2021.
- [36] S. Tulyakov, A. Bochicchio, D. Gehrig, S. Georgoulis, Y. Li, and D. Scaramuzza, “Time lens++: Event-based frame interpolation with parametric non-linear flow and multi-scale fusion,” *IEEE Conference on Computer Vision and Pattern Recognition (CVPR)*, 2022.
- [37] —, “Time lens++: Event-based frame interpolation with parametric non-linear flow and multi-scale fusion,” *IEEE Conference on Computer Vision and Pattern Recognition (CVPR)*, 2022.
- [38] R. Zou, M. Muglikar, N. Messikommer, and D. Scaramuzza, “Seeing behind dynamic occlusions with event cameras,” 2023.
- [39] J. Wang, W. Weng, Y. Zhang, and Z. Xiong, “Unsupervised video deraining with an event camera,” in *Proceedings of the IEEE/CVF International Conference on Computer Vision (ICCV)*, October 2023, pp. 10 831–10 840.
- [40] A. Photoshop, <https://www.adobe.com/products/photoshop.html>.
- [41] A. Paszke, S. Gross, F. Massa, A. Lerer, J. Bradbury, G. Chanan, T. Killeen, Z. Lin, N. Gimelshein, L. Antiga, A. Desmaison, A. Kopf, E. Yang, Z. DeVito, M. Raison, A. Tejani, S. Chilamkurthy, B. Steiner, L. Fang, J. Bai, and S. Chintala, “Pytorch: An imperative style, high-performance deep learning library,” in *Advances in Neural Information Processing Systems*, H. Wallach, H. Larochelle, A. Beygelzimer, F. d’Alché-Buc, E. Fox, and R. Garnett, Eds., vol. 32. Curran Associates, Inc.,

2019. [Online]. Available: [https://proceedings.neurips.cc/paper\\_files/paper/2019/file/bdbca288fee7f92f2bfa9f7012727740-Paper.pdf](https://proceedings.neurips.cc/paper_files/paper/2019/file/bdbca288fee7f92f2bfa9f7012727740-Paper.pdf)
- [42] D. P. Kingma and J. Ba, "Adam: A method for stochastic optimization," *CoRR*, vol. abs/1412.6980, 2014. [Online]. Available: <https://api.semanticscholar.org/CorpusID:6628106>
- [43] H. Rebecq, R. Ranftl, V. Koltun, and D. Scaramuzza, "High speed and high dynamic range video with an event camera," *IEEE Trans. Pattern Anal. Mach. Intell.*, 2019.
- [44] B. Li, W. Ren, D. Fu, D. Tao, D. Feng, W. Zeng, and Z. Wang, "Benchmarking single-image dehazing and beyond," *IEEE Transactions on Image Processing*, vol. 28, no. 1, pp. 492–505, 2018.
- [45] R. Ranftl, A. Bochkovskiy, and V. Koltun, "Vision transformers for dense prediction," *ArXiv preprint*, 2021.
- [46] B. Li, W. Ren, D. Fu, D. Tao, D. Feng, W. Zeng, and Z. Wang, "Benchmarking single-image dehazing and beyond," *Trans. Img. Proc.*, vol. 28, no. 1, p. 492–505, Jan. 2019. [Online]. Available: <https://doi.org/10.1109/TIP.2018.2867951>
- [47] T. Delbruck, Y. Hu, and Z. He, "V2E: From video frames to realistic DVS event camera streams," *arXiv e-prints*, 2020.
- [48] T. Finateu, A. Niwa, D. Matolin, K. Tsuchimoto, A. Mascheroni, E. Reynaud, P. Mostafalu, F. Brady, L. Chotard, F. LeGoff, H. Takahashi, H. Wakabayashi, Y. Oike, and C. Posch, "A 1280x720 back-illuminated stacked temporal contrast event-based vision sensor with 4.86 $\mu$ m pixels, 1.066geps readout, programmable event-rate controller and compressive data-formatting pipeline," in *IEEE Intl. Solid-State Circuits Conf. (ISSCC)*, 2020.
- [49] Z. Teed and J. Deng, "RAft: Recurrent All-Pairs Field Transforms for Optical Flow," in *Eur. Conf. Comput. Vis. (ECCV)*, 2020.
- [50] T. Brödermann, D. Bruggemann, C. Sakaridis, K. Ta, O. Liagouris, J. Corkill, and L. Van Gool, "Muses: The multi-sensor semantic perception dataset for driving under uncertainty," *arXiv preprint arXiv:2401.12761*, 2024.
- [51] M. Muglikar, S. Somasundaram, A. Dave, E. Charbon, R. Raskar, and D. Scaramuzza, "Event cameras meet spads for high-speed, low-bandwidth imaging," 2025, pp. 1–12.